Object Contour Reconstruction using Bio-inspired Sensors

Christoph Will[1], Joachim Steigenberger[2] and Carsten Behn[1]
[1]*Department of Technical Mechanics, Technische Universität Ilmenau, Max-Planck-Ring 12 (Building F), 98693 Ilmenau, Germany*
[2]*Institute of Mathematics, Technische Universität Ilmenau, Weimarer Straße 25, 98693 Ilmenau, Germany*

Keywords: Vibrissa, Mechanical Contact, Beam, Bending, Large Deflections, Profile Reconstruction.

Abstract: This work is inspired and motivated by the sophisticated mammals sense organ of touch: vibrissa. Mammals, especially rodents, use their vibrissae, located in the snout region – mystacial vibrissae – to determine object contacts (passive mode) or to scan object surfaces (active mode). Here, we focus on the passive mode. In order to get hints for an artificial sensing prototype, we set up a mechanical model in form of a long slim beam which is one-sided clamped. We investigate in a purely analytical way a quasi-static sweep of the beam along a given profile, where we assume that the profile boundary is strictly convex. This sweeping procedure shows up in two phases, which have to be distinguished in profile contact with the tip and tangentially contact (between tip and base). The analysis eventuates in a phase decision criterion and in a formula for the contact point. These are the main results. Moreover, based on the observables of the problem, i.e. the clamping moment and the clamping forces, which are the only information the animal relies on, a reconstruction of the profile is possible – even with added uncertainty mimicking noise in experimental data.

1 INTRODUCTION

Rodents, like mice and rats, use tactile hairs in the snout region (mystacial vibrissae) to obtain information about the environment, whereby these vibrissae are used in an active and passive mode. The vibrissae are supported in a compliant follicle sine complex (FSC) as shown in Figure 1. The follicle sine complex exhibits a large variety of mechanoreceptors, like merkel cells, which detect the movement of the vibrissa base and convert this mechanical strain into signals to the central nervous system.

The main difficulty is the fact, that the animals get only information about the environment from the processing mechanoreceptors.

Inspired by this biological paragon and motivated by its complex task to govern information, we focus on a vibrissa in passive mode, i.e., object localization. We set up a mechanical model in form of a plane elastic bending rod for a quasi-static object scanning. The exploitation of the corresponding mathematical model is primarily not based on numerical methods, but it relies on an analytical framework as far as possible. Before doing this, we focus on the state of art to make a dissociation of the actual work in this field.

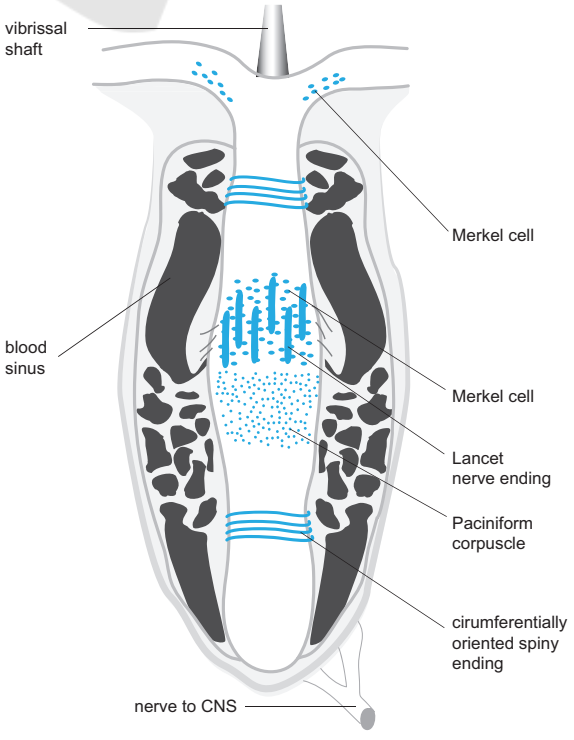

Figure 1: Follicle sine complex (Behn, 2013b), arranged by D. Voges (TU Ilmenau).

Will C., Steigenberger J. and Behn C..
Object Contour Reconstruction using Bio-inspired Sensors.
DOI: 10.5220/0005018004590467
In *Proceedings of the 11th International Conference on Informatics in Control, Automation and Robotics* (ICINCO-2014), pages 459-467
ISBN: 978-989-758-039-0

2 STATE OF THE ART

Various approaches are done in literature to model the biological paragon to get hints for a technical implementation in, e.g., robotics for obstacle detection (Kim and Möller, 2006), (Pearson et al., 2011), (Prescott et al., 2009).

First models, like the one presented in (Hirose et al., 1989), consider long thin elastic beams for detection of deformation caused by an obstacle contact. If this "whisker-like" sensor perceives a deformation of the beam (which has to be sufficiently large as to exceed some given threshold), the actual position is marked for further trajectory planning. Hence, the pure existence of an obstacle is needed, no other information about the obstacle is requested (just detection).

Further approaches are given in (Kim and Möller, 2007) and (Tuna et al., 2012), which realize additional information about the obstacle. In (Tuna et al., 2012), a contact point with an obstacle is estimated using the angle of deflection at the base (inspired by methods in computer tomography, ray deflection). The authors in (Kim and Möller, 2007) use the linear theory of elasticity in application to large deflections of a beam. In both methods, only the angle of deflection, neither forces nor moments, are measured.

In (Birdwell et al., 2007), another model is given which incorporates both small deformations and the pre-curvature of the beam. This is done in adding the pre-curvature to the linear deflection of the beam to get the actual position of the beam. The achievable accuracy of the model depends on the pre-curvature of the beam, because the curvature is assumed to be a function on the beam axis. For small radii of sufficiently long beams, this method can fail due to the cartesian coordinate system. Also, it is still unclear, if the pre-curvature of the vibrissa results in a pre-stress.

An improved method for object localization and shape detection is proposed in (Scholz and Rahn, 2004) for plane problems, in (Clements and Rahn, 2006) for spatial problems. In both works, the authors switch from linear approximation of the curvature to the description of the problem in natural coordinates. This is a main improvement in comparison to works presented above. Thus, they allow for large deflections of the beam, which results in a clear formulation of the boundary conditions. Further, experimental data are used in a numerical reconstruction algorithm in Simulink which results in the deformed beam shapes and a numerical values for the contact point. The entirety of all these beam shapes models the shape of the object geometry.

Recent works, like (Pammer et al., 2013), approximate the curvature of the beam in using finite differences. This gives the possibility to consider the curvatures of an undeformed vibrissa, but analytical equations with new insights do not exist due to numerical simulations.

3 AIM AND SCOPE

In this paper, due to Section 2, we focus on an entire analytical treatment of the scanning problem of an obstacle via a beam vibrissa. Since we have to allow for large deflections of the beam, we introduce the nonlinear Euler-Bernoulli theory of beam bending. Moreover, we set up a mechanical model and investigate the quasi-static bending behavior, when the beam is swept along an obstacle. In order to get information about the obstacle, we determine both forces and moments at the base (here: a clamping of the beam) as solutions of a boundary value problem (BVP). Reversely, we use them in an initial value problem (IVP) to determine a contact point of the deformed beam with the obstacle. The series of all contact points exhibit the shape of the obstacle.

4 MODELING

The present paper deals with the problem what an animal "feels" and perceives by means of a single vibrissa while moving along an obstacle, and which information it can get about the obstacle. As already mentioned in Section 1, the only information is available at the support of the vibrissa.

4.1 Assumptions

In order to get further information, we treat the problem analytically to the greatest extent. The work is based on (Steigenberger, 2013) and (Will, 2013). In order to model the problem, the following assumptions are made:

- The problem is treated as a quasi-static one.
- We restrict the problem to an (x,y)-plane. The (originally undeformed) vibrissa is vertical, its base moves along the x-axis from the right to the left.
- The vibrissa is assumed as a long, slim, straight (until now, no pre-curvature is assumed) beam with constant second moment of area I_z, constant Young's modulus E and length L. Thus, ignoring shear stress, the Euler-Bernoulli theory for large deflections is applicable.

- The stress of the beam is sufficiently small to use Hooke's law of linear elasticity.
- The support of the beam is a clamp.
  Clearly, this does not match the reality of the vibrissa. In further works, we take a glimpse to an elastic support due to the compliant properties of the FSC, see Figure 1.
- The obstacle contour (i.e., its boundary) is a strictly convex function $g : x \mapsto g(x)$, with $g \in \mathcal{C}^1(\mathbb{R};\mathbb{R})$.
- The object contact is ideal, i.e., the deformation of the beam is caused by a single contact force perpendicular to the obstacle profile. Friction is not taken into account.

4.2 Model

The starting point is

$$\kappa(s) = \frac{M_{bz}(s)}{EI_z}, \tag{1}$$

which is valid due to the assumptions in Section 4.1. Here, $M_{bz}(\cdot)$ denotes the bending moment with respect to the z-axis, $s \in [0, L]$ is the arc length of the beam, and $\kappa(\cdot)$ represents the curvatures, see Figure 2. For the sake of brevity, we introduce dimensionless variables. The units of measure are $[\text{length}] = L$, $[\text{moments}] = EI_zL^{-1}$ and $[\text{forces}] = EI_zL^{-2}$ (for example: $s = Ls^*$, $s^* \in [0,1]$).

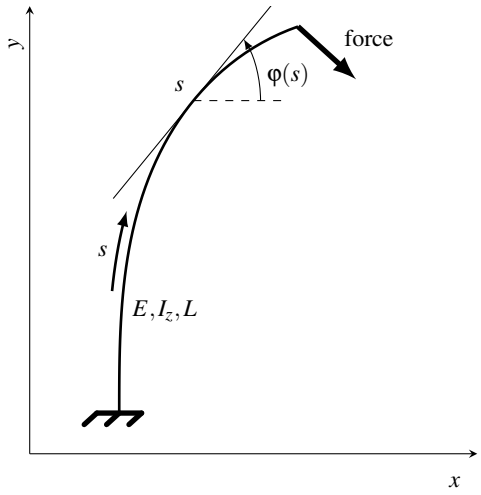

Figure 2: Euler-Bernoulli beam under large deflection.

As from now, all quantities are given in dimensionless representation, whereby the asterisk is dropped. Then, (1) becomes

$$\kappa(s) = M_{bz}(s) \tag{2}$$

and the deformed beam is described by

$$\left.\begin{aligned} \frac{\mathrm{d}}{\mathrm{d}s}x(s) &= \cos\left(\varphi(s)\right), \\ \frac{\mathrm{d}}{\mathrm{d}s}y(s) &= \sin\left(\varphi(s)\right), \\ \frac{\mathrm{d}}{\mathrm{d}s}\varphi(s) &= \kappa(s), \end{aligned}\right\}$$

with initial conditions $x(0) = x_0$, $y(0) = 0$ and $\varphi(0) = \frac{\pi}{2}$ (due to the clamping). Because of the strict convexity of g, x and y are functions of the slope angle α:

$$\begin{aligned} & \frac{\mathrm{d}}{\mathrm{d}x}g(x) = g'(x) = \tan(\alpha) \\ \Rightarrow \quad & x = \xi(\alpha) := g'^{-1}(\tan(\alpha)), \\ \Rightarrow \quad & y = \eta(\alpha) := g(\xi(\alpha)). \end{aligned}$$

Now:

$$\big(x, g(x)\big) \mapsto \big(\xi(\alpha), \eta(\alpha)\big).$$

To formulate the boundary conditions, we have to distinguish two configurations of contacting the profile, see Figure 3:

- Phase A: Contact of beam tip and profile with $\varphi(1) \geq \alpha$,
- Phase B: Contact of a point $s_1 \in (0,1)$ and the profile with equal angles $\varphi(s_1) = \alpha$.

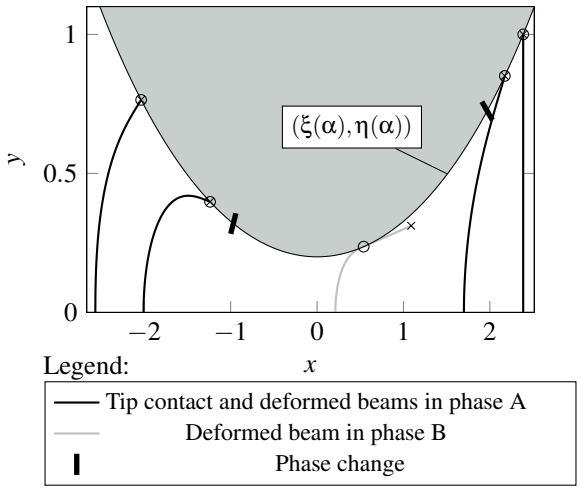

Figure 3: Profile with deflected beams.

In both phases, the contact point is given by the slope angle α of the profile.

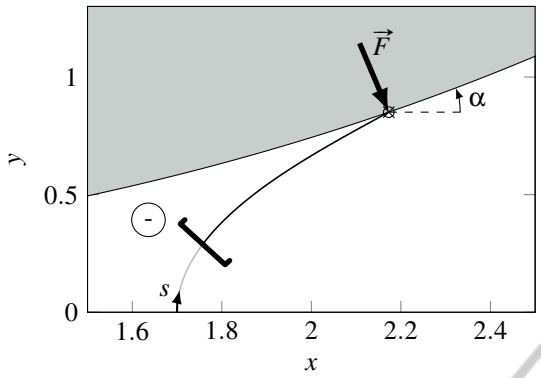

Figure 4: Deflected beam in Phase A.

4.3 Phase A: Contact at the Tip

Using Figure 4, the bending moment is for $s \in (0,1)$:

$$M_{bz}(s) = f\Big(\big(y(s)-\eta(\alpha)\big)\sin(\alpha) + \big(x(s)-\xi(\alpha)\big)\cos(\alpha)\Big), \tag{3}$$

Decoupling of the bending moment from $x(s)$ and $y(s)$, the derivative of (3) yields the following ODE system (4) with boundary conditions (5):

$$\begin{array}{ll} \text{(a)}\ \ \kappa'(s) = f\cos(\varphi(s)-\alpha) & \text{(c)}\ \ x'(s) = \cos(\varphi(s)) \\ \text{(b)}\ \ \varphi'(s) = \kappa(s) & \text{(d)}\ \ y'(s) = \sin(\varphi(s)) \end{array} \tag{4}$$

$$\begin{array}{llll} \text{(a)}\ \ \varphi(0) = \frac{\pi}{2} & & \text{(d)}\ \ x(1) = \xi(\alpha) \\ \text{(b)}\ \ y(0) = 0 & \text{(c)}\ \ \kappa(1) = 0 & \text{(e)}\ \ y(1) = \eta(\alpha) \end{array} \tag{5}$$

This BVP splits into two separate problems: {(4a,b),(5a,c)} and {(4c,d),(5b,d,e)}. The first one has

$$\kappa^2 = 2f\left(\sin(\varphi-\alpha) - \sin(\varphi_1-\alpha)\right) \tag{6a}$$

$$= 4f\sin\left(\frac{\varphi-\varphi_1}{2}\right)\cos\left(\frac{\varphi+\varphi_1-2\alpha}{2}\right). \tag{6b}$$

as a first integral with $\varphi_1 := \varphi(1)$.

Remark 4.1. *The bending moment, considering the lower part of the beam, depends on the clamp reactions M_{Az}, F_{Ax}, F_{Ay}, which results in a first integral of the form:*

$$\kappa^2 = 2f\sin(\varphi-\alpha) - 2f\cos(\alpha) + M_{Az}^2.$$

Because $\kappa^2(s) \geq 0$ has to be fulfilled, three cases have to be discussed for (6b) with $f > 0$:

1. At least one factor is zero: hence $\kappa(s) \equiv 0$, and the beam is not deformed at all.
2. Both factors are negative: The sine function is positive on the interval $(-\pi, 0)$ and negative on $(\pi, 2\pi)$. This results in the inequations
   $-2\pi < \varphi(s) - \varphi_1 < 0 \quad \vee \quad 2\pi < \varphi(s) - \varphi_1 < 4\pi$.
   Hence $\varphi(s) < \varphi_1 \ \vee\ \varphi(s) > 2\pi$. This is a **contradiction**, because $\varphi(s) \in \left[\varphi_1, \frac{\pi}{2}\right]\ \forall s \in [0,1]$.
3. Both factors are positive: The sine function is positive on the domain $(0,\pi)$, the cosine function on $\left(-\frac{\pi}{2}, \frac{\pi}{2}\right)$. Therefore, it must hold:
   $0 < \varphi(s) - \varphi_1 < 2\pi \ \wedge\ -\pi < \varphi(s) + \varphi_1 - 2\alpha < \pi$.
   The first inequality contains no additional information, the second one yields:
   $$\varphi(s) + \varphi_1 < \pi + 2\alpha\ \forall s$$
   $$\Rightarrow \qquad \varphi_1 < \frac{\pi}{2} + 2\alpha, \ \text{ since } \ \varphi(s) \leq \frac{\pi}{2}.$$
   Therefore, the angle φ_1 has to be in the domain $\alpha < \varphi_1 < \min\left(\left\{\frac{\pi}{2}, \frac{\pi}{2} + 2\alpha\right\}\right)$.

Due to the assumptions, the curvature is non-positive along the solutions of (4a,b), which results in, using (6a):

$$\frac{\mathrm{d}\varphi(s)}{\mathrm{d}s} = \kappa(s) = -\sqrt{2f\left(\sin(\varphi(s)-\alpha) - \sin(\varphi_1-\alpha)\right)} \tag{7}$$

as a ODE with separated variables for $\varphi(s)$. Introducing $\mathbb{H}_A$:

$$\mathbb{H}_A : (t,u) \mapsto \mathbb{F}\left(\frac{\sin\left(\frac{\pi}{4} - \frac{t}{2}\right)}{\sin\left(\frac{\pi}{4} - \frac{u}{2}\right)}, \sin\left(\frac{\pi}{4} - \frac{u}{2}\right)\right), \tag{8}$$

where $\mathbb{F}$ is the incomplete elliptic integral of first kind according to the definition (Abramowitz and Stegun, 1972, 17.2.7)

$$\mathbb{F} : (z,k) \mapsto \int_0^z \frac{1}{\sqrt{1-\psi^2}\sqrt{1-k^2\psi^2}}\,\mathrm{d}\psi,$$

the separation of variables applied on (7) with initial value (5a) yields:

$$\sqrt{f}s = \mathbb{H}_A\left(\varphi(s)-\alpha, \varphi_1-\alpha\right) - \mathbb{H}_A\left(\frac{\pi}{2}-\alpha, \varphi_1-\alpha\right). \tag{9}$$

Hence, the contact force f can be expressed as

$$f(\varphi_1,\alpha) := \left(\mathbb{H}_A\left(\varphi_1-\alpha, \varphi_1-\alpha\right) - \mathbb{H}_A\left(\frac{\pi}{2}-\alpha, \varphi_1-\alpha\right)\right)^2. \tag{10}$$

Now, the only unknown parameter at this stage is the angle φ_1 at the tip. To determine this parameter, (5b,e) have to be used in the following two ways.

4.3.1 Substitution of Variable

Here, y is given in dependence on φ:

$$\frac{\frac{\mathrm{d}y(s)}{\mathrm{d}s}}{\frac{\mathrm{d}\varphi(s)}{\mathrm{d}s}} = \frac{\mathrm{d}y(\varphi)}{\mathrm{d}\varphi} = \frac{1}{\kappa(\varphi)}\sin(\varphi)\,,$$

with boundary conditions $y(\frac{\pi}{2}) = 0$ and $y(\varphi_1) = \eta(\alpha)$. At first, the first condition leads to

$$y(\varphi) = -\frac{1}{\sqrt{2f}}\int_{\frac{\pi}{2}}^{\varphi} \frac{\sin(\tau)}{\sqrt{\sin(\tau-\alpha)-\sin(\varphi_1-\alpha)}}\,\mathrm{d}\tau.$$

The second boundary condition results in an implicit expression for $\varphi_1 \in \left(\alpha, \min\left\{\frac{\pi}{2}, \frac{\pi}{2}+2\alpha\right\}\right)$:

$$\eta(\alpha)\sqrt{2f} + \int_{\frac{\pi}{2}}^{\varphi_1} \frac{\sin(\tau)}{\sqrt{\sin(\tau-\alpha)-\sin(\varphi_1-\alpha)}} = 0. \tag{11}$$

Note that the integral (11) can be represented by means of elliptic integrals and solved for φ_1.

4.3.2 Shooting Method

Instead of substituting the variable, the problem can efficiently be solved by applying a shooting method for φ_1, which can be both faster and more accurate.

Let $\varphi_1^* \in \left[\alpha+\varepsilon, \min\left\{\frac{\pi}{2}, \frac{\pi}{2}+2\alpha\right\}-\varepsilon\right]$ be a valid candidate for φ_1. The corresponding deflection angle $\varphi(s)$ can be calculated from (9) using (10):

$$\varphi(s,\varphi_1^*) = \alpha + \mathbb{H}_A^{-1}\left(\sqrt{f(\varphi_1^*,\alpha)}s + \mathbb{H}_A\left(\frac{\pi}{2}-\alpha, \varphi_1^*-\alpha\right), \varphi_1^*-\alpha\right),$$

with

$$\mathbb{H}_A^{-1}(t,u) := -\frac{\pi}{2} + 2\arccos\left(\mathrm{JacobiSN}\left(t, \cos\left(\frac{\pi}{4}+\frac{u}{2}\right)\right)\cos\left(\frac{\pi}{4}+\frac{u}{2}\right)\right)$$

from (8) and JacobiSN according to (Abramowitz and Stegun, 1972, 16.1.3 and 16.1.5).

Now (4d) with (5b) yield

$$y(s,\varphi_1^*) = \int_0^s \sin(\varphi(\tau,\varphi_1^*))\,\mathrm{d}\tau,$$

which can be numerically computed. The shooting value for φ_1^* is correct, if $y(1,\varphi_1^*) - \eta(\alpha) = 0$.

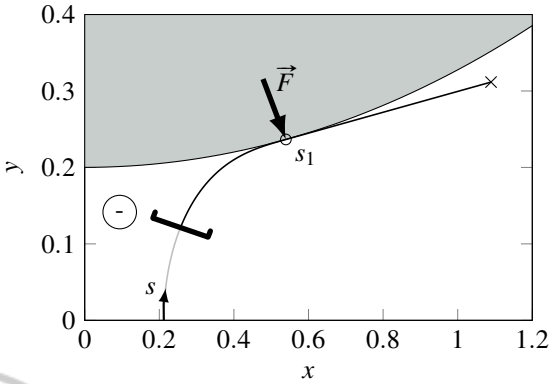

Figure 5: Deflected beam in Phase B, contact $s_1 \in (0,1)$.

Summarizing, independent of the chosen method, φ_1 is now known. The solution of (4c,d) is:

$$x = \xi(\alpha) + \int_1^s \cos(\varphi(\tau))\,\mathrm{d}\tau, \tag{12}$$

$$y = \eta(\alpha) + \int_1^s \sin(\varphi(\tau))\,\mathrm{d}\tau.$$

4.4 Phase B: Tangential Contact

The bending moment is now, with yet unknown contact point s_1 (see Figure 5):

$$M_{bz}(s) = \begin{cases} f\Big(\big(y(s)-\eta(\alpha)\big)\sin(\alpha) \\ \quad +\big(x(s)-\xi(\alpha)\big)\cos(\alpha)\Big) & ,s \in (0,s_1] \\ 0 & ,s \in (s_1,1)\,. \end{cases} \tag{13}$$

The related BVP with $s \in (0,s_1)$ is:

(a)	$\kappa'(s) = f\cos(\varphi(s)-\alpha)$	(c)	$x'(s) = \cos(\varphi(s))$
(b)	$\varphi'(s) = \kappa(s)$	(d)	$y'(s) = \sin(\varphi(s))$

(14)

(a)	$\varphi(0) = \frac{\pi}{2}$	(c)	$\kappa(s_1) = 0$	(e)	$x(s_1) = \xi(\alpha)$
(b)	$y(0) = 0$	(d)	$\varphi(s_1) = \alpha$	(f)	$y(s_1) = \eta(\alpha)$

(15)

A first integral of (14a) together with (14b) and (15c) is

$$\kappa^2 = 2f\sin(\varphi-\alpha)$$

$$\Rightarrow \quad \frac{\mathrm{d}}{\mathrm{d}s}\varphi(s) = \kappa(s) = -\sqrt{2f}\sqrt{\sin(\varphi(s)-\alpha)}\,. \tag{16}$$

Equation (14b) with (16) and (15a) yield

$$\sqrt{f}s = \mathbb{H}_B(\varphi(s)-\alpha) - \mathbb{H}_B\left(\frac{\pi}{2}-\alpha\right),$$

which can be solved for $\varphi(s)$:

$$\varphi(s) = \alpha + \mathbb{H}_B^{-1}\left(\sqrt{f}s + \mathbb{H}_B\left(\frac{\pi}{2}-\alpha\right)\right),$$

using

$$\mathbb{H}_B : t \to \mathbb{F}\left(\sqrt{2}\sin\left(\frac{\pi}{4}-\frac{t}{2}\right), \frac{\sqrt{2}}{2}\right),$$

with

$$\mathbb{H}_B^{-1}(t) = -\frac{\pi}{2} + 2\arccos\left(\frac{\sqrt{2}}{2}\,\text{JacobiSN}\left(t, \frac{\sqrt{2}}{2}\right)\right).$$

Since $\varphi(s_1) = \alpha$ is known, the contact force can be expressed as

$$\sqrt{f} = \frac{\mathbb{H}_B(0) - \mathbb{H}_B\left(\frac{\pi}{2}-\alpha\right)}{s_1}. \quad (17)$$

Again, considering the function y to get the last missing parameter s_1, condition (15b) results in:

$$y(s) = \frac{1}{\sqrt{f}} \int_{\mathbb{H}_B\left(\frac{\pi}{2}-\alpha\right)}^{\sqrt{f}s+\mathbb{H}_B\left(\frac{\pi}{2}-\alpha\right)} \sin\left(\alpha + \mathbb{H}_B^{-1}(\tau)\right) d\tau. \quad (18)$$

Summarizing, (17), (18) and (15f) yield

$$f(\alpha) = \left(\frac{1}{\eta(\alpha)} \int_{\mathbb{H}_B\left(\frac{\pi}{2}-\alpha\right)}^{\mathbb{H}_B(0)} \sin\left(\alpha + \mathbb{H}_B^{-1}(\tau)\right) d\tau\right)^2. \quad (19)$$

Now, (17) and (19) lead to the following equation for the contact point s_1:

$$s_1(\alpha) = \frac{\eta(\alpha)\left(\mathbb{H}_B(0) - \mathbb{H}_B\left(\frac{\pi}{2}-\alpha\right)\right)}{\int_{\mathbb{H}_B\left(\frac{\pi}{2}-\alpha\right)}^{\mathbb{H}_B(0)} \sin\left(\alpha + \mathbb{H}_B^{-1}(\tau)\right) d\tau}. \quad (20)$$

The last integral of (14c) with (15e) is:

$$x(s) = x_0 + \frac{1}{\sqrt{f}} \int_{\mathbb{H}_B\left(\frac{\pi}{2}-\alpha\right)}^{\sqrt{f}s+\mathbb{H}_B\left(\frac{\pi}{2}-\alpha\right)} \cos\left(\alpha + \mathbb{H}_B^{-1}(\tau)\right) d\tau,$$

whence, with $s = s_1$, we obtain the foot coordinate

$$x_0 = \xi(\alpha) - \frac{1}{\sqrt{f}} \int_{\mathbb{H}_B\left(\frac{\pi}{2}-\alpha\right)}^{\mathbb{H}_B(0)} \cos\left(\alpha + \mathbb{H}_B^{-1}(\tau)\right). \quad (21)$$

Finally, for both phases, the footpoint x_0 is derived using (12) and (21). Using (10) and (19) we can determine f and, hence, knowing α, also the contact force $\vec{F}$. With f we get the clamping forces F_{Ax} and F_{Ay}, as well as the clamping moment M_{Az} using (3) and (13).

5 SIMULATIONS

Let us focus on the following two profile functions:

$$g_1 : x \mapsto \frac{1}{2}x^2 + \frac{1}{2},$$

$$g_2 : x \mapsto \begin{cases} -\sqrt{2^2 - x^2} + \frac{5}{2}, & x > 0, \\ -\sqrt{\frac{1}{4} - x^2} + 1, & \text{else}. \end{cases}$$

Function g_1 is a parabola, and g_2 is a profile composed of two circles, both shown in Figure 6.

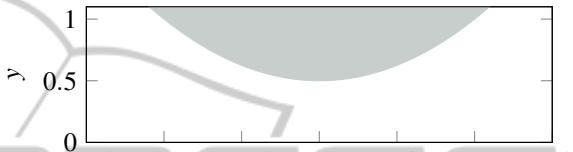

(a) Parabola profile g_1

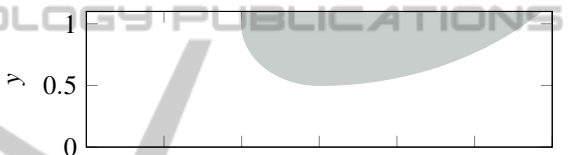

(b) Profile composed of two circles g_2

Figure 6: Profiles under consideration.

Computed observables for profile g_1 are exemplarily shown in Figure 7.

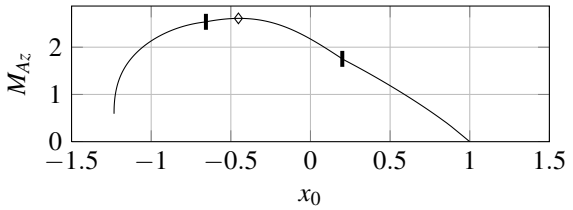

(a) Clamping moment M_{Az} (maximum marked with ◊)

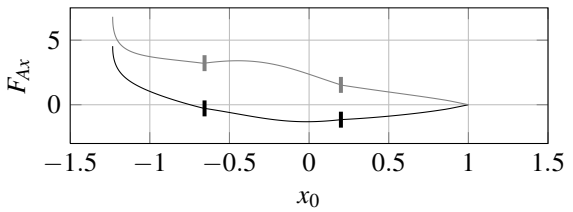

(b) Clamping forces F_A (—— F_{Ax}; —— F_{Ay})

Figure 7: Observables with profile function g_1. ❙ marks the change between Phase A and Phase B.

The maximum clamping moment occurs in Phase B, but besides a change of phase in M_{Az} and F_{Ay}. Obviously, no direct information about the obstacle can be extracted directly from the curve of the observables. We rather use the computed observables for an object profile reconstruction in the next section.

6 RECONSTRUCTION OF THE PROFILE

At this stage, we have the observables $x_0, F_{Ax}, F_{Ay}, M_{Az}$ (values which are assumed that an animal can solely rely on) numerically computed at hand. They represent the only information. In experiments these values are produced by a measurement device.

We have to focus on a reconstruction procedure of the obstacle profile, out of these "measured" values.

6.1 Analysis

Let us start with the following information at the base:

$$\begin{aligned}\kappa(0) &= \lim_{s\to 0+} M_{bz}(s) = -M_{Az}\,,\\ \varphi(0) &= \frac{\pi}{2}\,,\\ x(0) &= x_0\,,\\ y(0) &= 0\end{aligned}$$

and

$$\alpha = -\arctan\left(\frac{F_{Ax}}{F_{Ay}}\right), \quad f \quad = \sqrt{F_{Ax}^2 + F_{Ay}^2}\,.$$

The main difficulty is to decide which phase the beam actually undergoes. To solve this, let us focus on the curvature (in Phase A, Phase B, or somewhere):

$$\text{Ph. A: } \kappa_A^2(s) = 2f\left(\sin(\varphi(s)-\alpha) - \sin(\varphi_1-\alpha)\right), \tag{22}$$

$$\text{any } s\text{: } \kappa_R^2(s) = 2f\left(\sin(\varphi(s)-\alpha) - \cos(\alpha)\right) + M_{Az}^2, \tag{23}$$

$$\text{Ph. B: } \kappa_B^2(s) = 2f\sin(\varphi(s)-\alpha)\,. \tag{24}$$

Obviously, it is Phase B iff $\varphi_1 = \alpha$. Using (23), φ_1 can be determined by:

$$\varphi_1 = \alpha - \arcsin\left(\frac{M_{Az}^2 - 2f\cos(\alpha)}{2f}\right),$$

which results in the decision condition for Phase B with only known parameters:

$$\boxed{M_{Az}^2 - 2F_{Ay} = 0\,.} \tag{25}$$

If (25) is valid, the contact force is applied at $s_1 \in (0,1)$ which can be computed:

$$s_1 = \frac{\mathbb{H}_B(0) - \mathbb{H}_B\left(\frac{\pi}{2} - \alpha\right)}{\sqrt{f}}\,.$$

Else, if (25) does not hold, the contact force is applied at $s_1 = 1$.

Now, the IVP is solved numerically using MATLAB's variable order Adams-Bashforth-Moulton PECE solver:

$$\begin{aligned}\varphi'(s) &= -\sqrt{2f\sin(\varphi(s)-\alpha) - 2f\cos(\alpha) + M_{Az}^2}\,,\\ \varphi(0) &= \frac{\pi}{2}\,,\\ x'(s) &= \cos(\varphi(s))\,, \qquad x(0) = x_0\,,\\ y'(s) &= \sin(\varphi(s))\,, \qquad y(0) = 0\,,\end{aligned}$$

which results in the reconstructed contact point:

$$\xi(\alpha) = x(s_1),\ \eta(\alpha) = y(s_1)\,.$$

6.2 Numerics

During reconstruction, the error for each component point k along the profile function g, shown in Figure 8, is computed using the euclidian norm of the distance between the given and the reconstructed contact point:

$$\text{error} := \left\| \begin{pmatrix} x_k(s_{1k}) \\ y_k(s_{1k}) \end{pmatrix} - \begin{pmatrix} \xi(\alpha_k) \\ \eta(\alpha_k) \end{pmatrix} \right\|_2$$

with s_{1k} as reconstructed contact point, $(x_k(s), y_k(s))$ the reconstructed position of the beam in the plane and $(\xi(\alpha_k), \eta(\alpha_k))$ the given contact point for computing the observables.

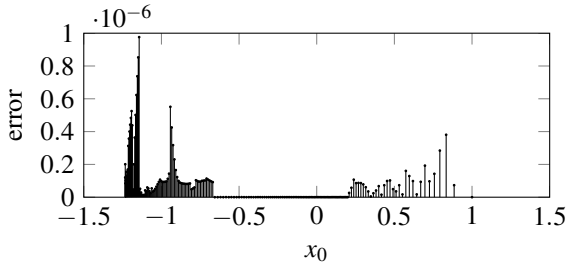

(a) Parabola profile g_1

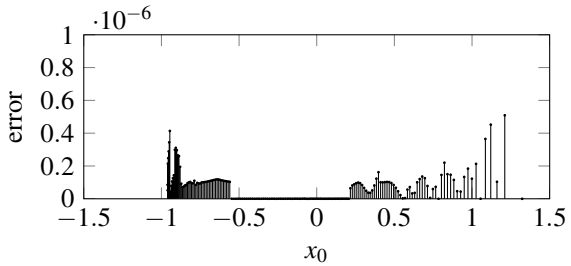

(b) Profile g_2

Figure 8: Reconstruction errors.

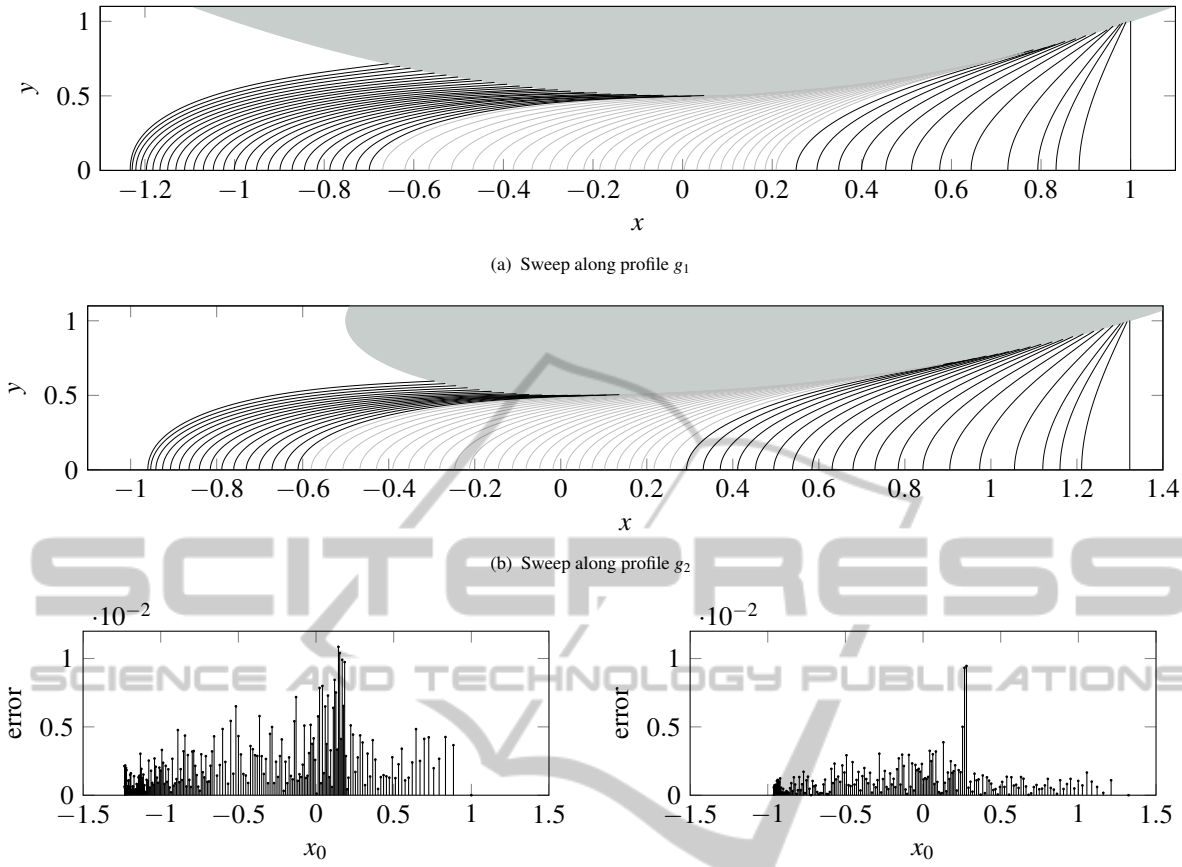

(a) Sweep along profile g_1

(b) Sweep along profile g_2

(c) Reconstruction error for profile g_1

(d) Reconstruction error for profile g_2

Figure 9: Reconstruction with added noise.

6.3 Reconstruction under Uncertainties

Because of lack of experiments, we assume that the computed observables underlie some measurement noise like in real experiments. To generate some noise to the observables, random uncertainty is added to F_{Ax}, F_{Ay} and M_{Az}. The scale of the added values is $\frac{1}{20}\left(\text{rnd}-\frac{1}{2}\right)$ for forces F_{Ax}, F_{Ay} and $\frac{1}{100}\left(\text{rnd}-\frac{1}{2}\right)$ for moment M_{Az}, $\text{rnd}\in(0,1)$ according to technical data sheet of a Schunk GmbH & Co. KG FT-Mini-40 force and moment sensor.

Besides the error obtained by the noisy observables, the decision if a tuple of observables belongs to Phase B or Phase A using (25) is very critical in the process of reconstruction. During the reconstruction using the computed observables, $\left|M_{Az}^2-2F_{Ay}\right|\leq 10^{-4}$ was used as condition for Phase B. With the added values, a higher tolerance gives better results, thus $\left|M_{Az}^2-2F_{Ay}\right|\leq 0.08$ was used. As shown in Figure 9(c) and (d), the reconstruction error is increased by four orders of magnitude if noise is added. For practical application, the profile is still sufficiently reconstructed as shown in Figure 9.

Clearly, the shape of the deformed vibrissa is an important part of the theory, but of little relevance in the result of the practical reconstruction process. The only important result is the sequence of the computed, reconstructed contact points of the profile.

7 CONCLUSION

Analytical investigations have shown that it is possible to reconstruct a profile contour by *one single sweep* of a thin elastic Euler-Bernoulli beam along it.

As a typical first step in modeling we determined the "observables" (reactions of the clamping), which an animal relies solely on, in a purely analytical way because of lack of experiments, in contrast to (Scholz and Rahn, 2004). But, the theoretical results showed up a single equation for a decision of the contact behavior of the beam with the object: contact at the tip, or contact between base and tip. This decision is new in literature and provides an easier and faster com-

putation of the deformed vibrissa and reconstruction of the profile as well. Furthermore, an explicit analytical formula to determine the contact point out of the "measured" values of the observables was derived. Both will increase the efficiency in experiments in future.

These results were obtained without assuming any estimation or approximation of describing functions. This is rather new in literature, in contrast to (Kim and Möller, 2007), (Birdwell et al., 2007).

Further on, to mimick experimental data, a reconstruction based solely on the "observables" with added random noise (uncertainty — mimicking noise in experiments) is valid for various profiles. But, obviously, the contact point approximation accuracy diminished from 10^{-6} to 10^{-2} (dimensionless), i.e., if the vibrissa is 1 m long then the obstacle contact position can be determined in the plane with an accuracy of 1 cm by a single measuring point during obstacle contour sensing. These results maintain the hypothesis from biologists, that animals can navigate by strongly relying on their mechanoreceptors at the FSC.

Near future (theoretical) work is addressed to the following investigations:

- analysis of the influence of an elastic support as in the biological paragon (Behn, 2013a): This could be needed to guarantee a bounded bending moment in controlling the support stiffness (i.e., the vibrissa does not brake during sensing – just think about a cat passing a fence).
- investigations on non-strictly convex profiles: There can appear flat points and we have to adjust our theory.
- switching from investigations in the vertical x-y-plane to a 3-dimensional sensing problem.

Intermediate future (experimental) work is addressed to experiments. At present, we are working on a design of a prototype for sensing obstacles.

Far future work is addressed to an application of such tactile sensors to mobile robotics (or a mouse-like robot) for online object localization and different tasks similar to the prototypes presented in (Kim and Möller, 2006) and (Pearson et al., 2011).

REFERENCES

Abramowitz, M. and Stegun, I. A. (1972). *Handbook of mathematical functions: With formulas, graphs, and mathematical tables*, volume 55 of *National Bureau of Standards applied mathematics series*. United States Department of Commerce, Washington, DC, 10. print., dec. 1972, with corr edition.

Behn, C. (2013a). *Mathematical Modeling and Control of Biologically Inspired Uncertain Motion Systems with Adaptive Features*. PhD thesis, Technische Universität Ilmenau, Ilmenau.

Behn, C. (2013b). Modeling the behavior of hair follicle receptors as technical sensors using adaptive control. In *ICINCO (1)*, pages 336–345.

Birdwell, J. A., Solomon, J. H., Thajchayapong, M., Taylor, M. A., Cheely, M., Towal, R. B., Conradt, J., and Hartmann, M. J. Z. (2007). Biomechanical Models for Radial Distance Determination by the Rat Vibrissal System. *Journal of Neurophysiology*, 98(4):2439–2455.

Clements, T. N. and Rahn, C. D. (2006). Three-dimensional contact imaging with an actuated whisker. *IEEE Transactions on Robotics*, 22(4):844–848.

Hirose, S., Inoue, S., and Yoneda, K. (1989). The whisker sensor and the transmission of multiple sensor signals. *Advanced Robotics*, 4(2):105–117.

Kim, D. and Möller, R. (2006). Passive sensing and active sensing of a biomimetic whisker. In Rocha, L. M., editor, *Artificial life X*, A Bradford book, pages 282–288. MIT Press, Cambridge, Mass.

Kim, D. and Möller, R. (2007). Biomimetic whiskers for shape recognition. *Robotics and Autonomous Systems*, 55(3):229–243.

Pammer, L., O'Connor, D. H., Hires, S. A., Clack, N. G., Huber, D., Myers, E. W., and Svoboda, K. (2013). The mechanical variables underlying object localization along the axis of the whisker. *The Journal of neuroscience : the official journal of the Society for Neuroscience*, 33(16):6726–6741.

Pearson, M. J., Mitchinson, B., Sullivan, J. C., Pipe, A. G., and Prescott, T. J. (2011). Biomimetic vibrissal sensing for robots. *Philosophical Transactions of the Royal Society B: Biological Sciences*, 366(1581):3085–3096.

Prescott, T., Pearson, M., Mitchinson, B., Sullivan, J. C. W., and Pipe, A. (2009). Whisking with robots: From Rat Vibrissae to Biomimetic Technology for Active Touch. *IEEE Robotics & Automation Magazine*, 16(3):42–50.

Scholz, G. R. and Rahn, C. D. (2004). Profile Sensing With an Actuated Whisker. *IEEE Transactions on Robotics and Automation*, 20(1):124–127.

Steigenberger, J. (2013). A continuum model of passive vibrissae.

Tuna, C., Solomon, J. H., Jones, D. L., and Hartmann, M. J. Z. (2012). Object shape recognition with artificial whiskers using tomographic reconstruction. In *IEEE International Conference on Acoustics, Speech and Signal Processing (ICASSP)*, pages 2537–2540, Piscataway, NJ. IEEE.

Will, C. (2013). *Anwendung nichtlinearer Biegetheorie auf elastische Balken zur Objektabtastung am Beispiel passiver Vibrissen mit unterschiedlicher Lagerung (Application of non-linear beam theory for obstacle detection with respect to the biological paragon of a passive vibrissa using different supports)*. Master thesis, Technische Universität Ilmenau, Ilmenau.